Molecular Cell, Volume *81*

Supplemental information

Gating movements and ion permeation in HCN4 pacemaker channels

Andrea Saponaro, Daniel Bauer, M. Hunter Giese, Paolo Swuec, Alessandro Porro, Federica Gasparri, Atiyeh Sadat Sharifzadeh, Antonio Chaves-Sanjuan, Laura Alberio, Giacomo Parisi, Gabriele Cerutti, Oliver B. Clarke, Kay Hamacher, Henry M. Colecraft, Filippo Mancia, Wayne A. Hendrickson, Steven A. Siegelbaum, Dario DiFrancesco, Martino Bolognesi, Gerhard Thiel, Bina Santoro, and Anna Moroni

Supplemental Information

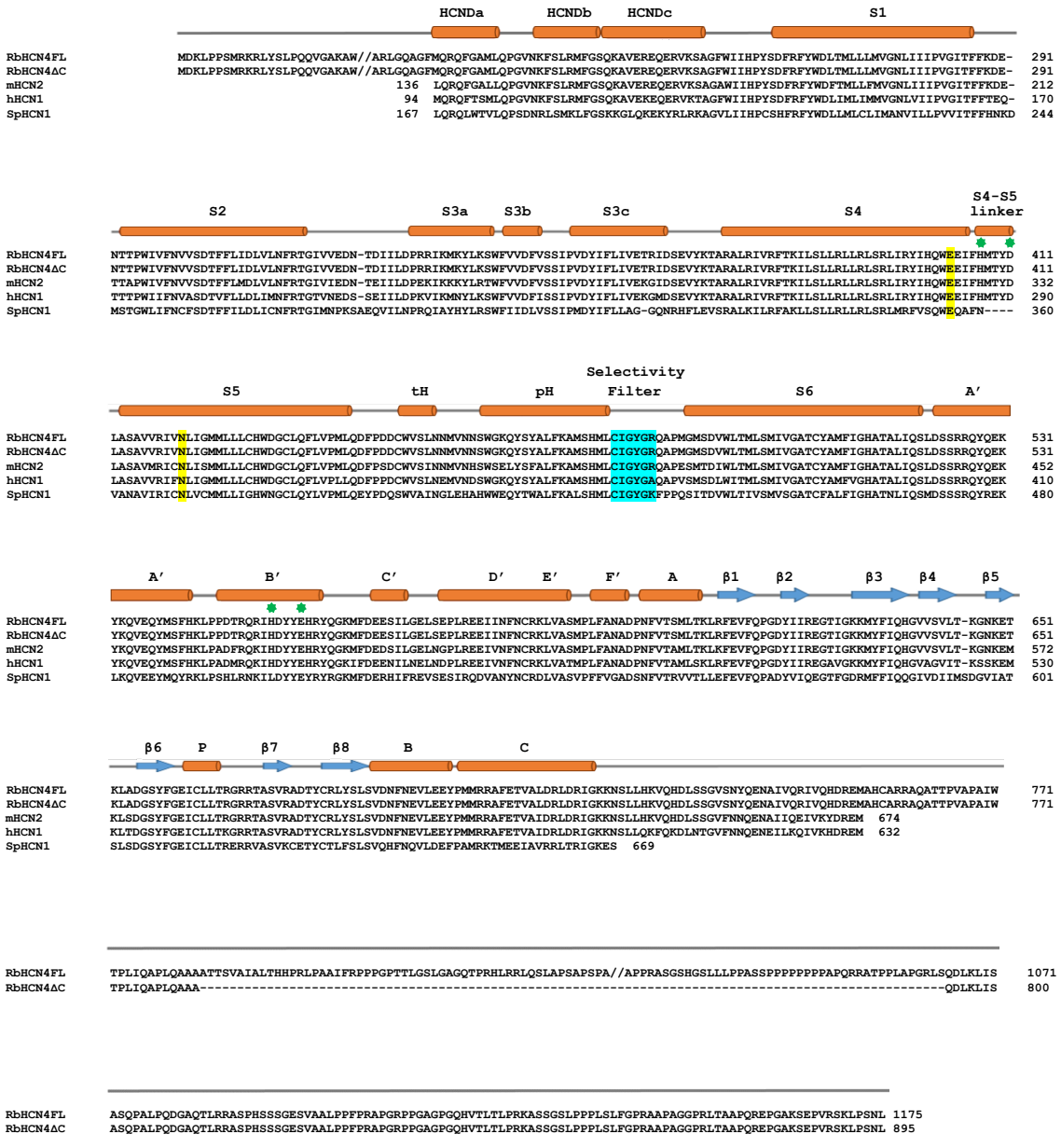

Figure S1: Sequence alignment and secondary structure elements of HCN channels (related to Figures 1,2 and 4)

Full-length rabbit HCN4 (RbHCN4FL), RbHCN4ΔC and the structured regions of mouse HCN2 (mHCN2), human HCN1 (hHCN1) and sea urchin HCN1 (SpHCN1) are aligned and shown. Secondary structures are represented by cilinders (α-helices, orange), arrows (β-strands, blue), and lines (loops, grey). Selectivity filter residues are highlighted (light blue). Residues forming a polar contact between S4 (E403) and S5 (N421) are highlighted (yellow). The four residues forming the metal ion coordination site are marked with asterisks (green). Parts of rabbit HCN4 sequence at the N- and C-termini have been omitted (shown by //). Amino acid sequence entries from UniProt databank are: RbHCN4, Q9TV66; mHCN2, O88703; hHCH1, O60741; SpHCN1, O76977.

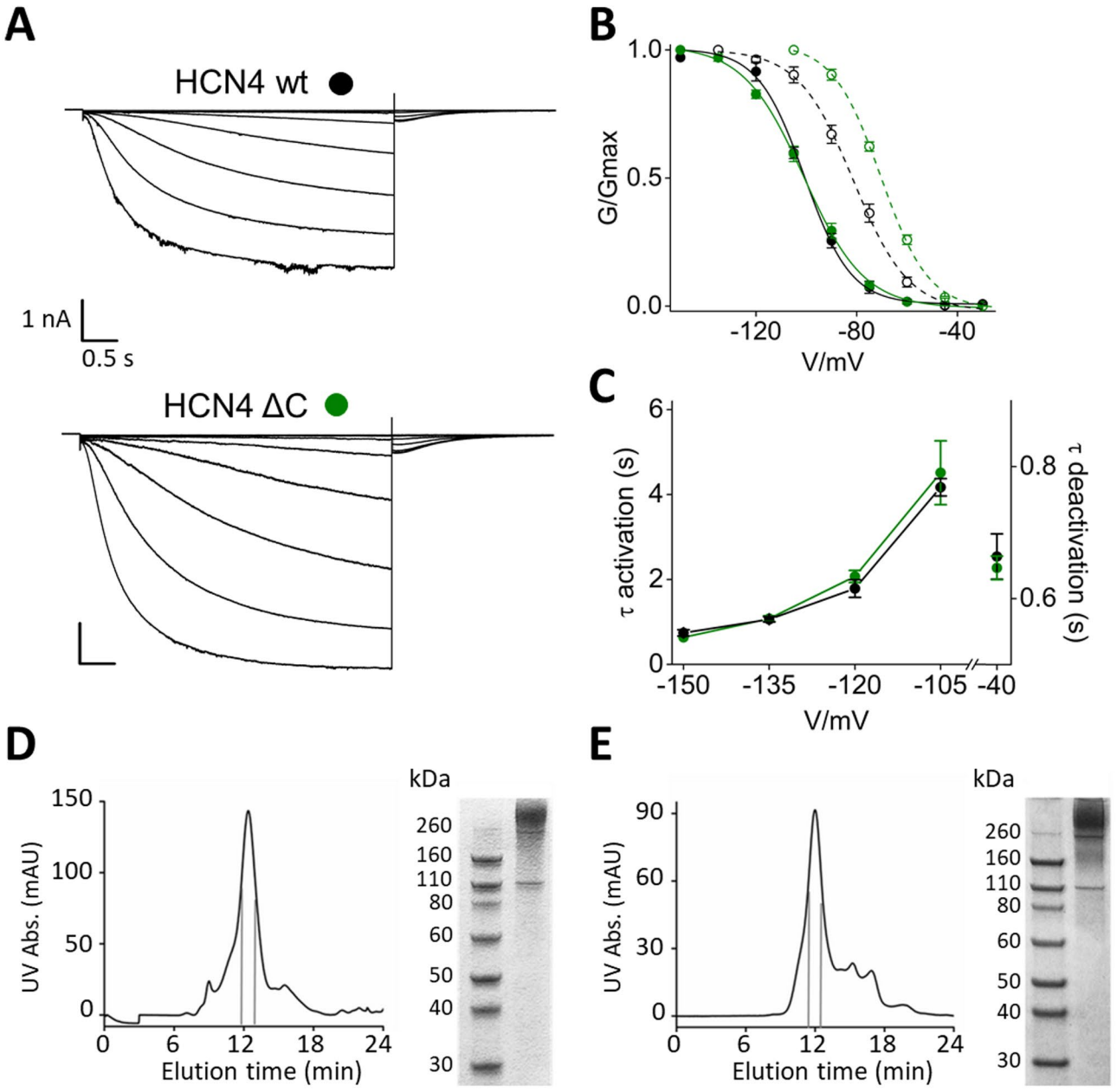

Figure S2: Functional and biochemical characterization of HCN4 ΔC construct (related to Figures 1,2,3 and 4)

A, Representative whole-cell currents of HCN4 wt and HCN4 ΔC recorded from -30 to -150 mV with -15mV increment. Scale bar: 500 ms x 1 nA. **B**, Mean tail current activation curves of wt (black) and ΔC (green) channels in control solution (filled symbols) and in the presence (empty symbols) of 30μM cAMP. Solid lines show Boltzmann fitting to the data (see STAR Methods). Values are reported in Table S1. **C**, Mean activation, and deactivation time constants (before and after the X axis, respectively) of wt (black) and ΔC (green) HCN4 channels. Values are reported in Table S2. **D**, Representative size-exclusion chromatography (SEC) of GFP-HCN4ΔC following purification in LMNG/CHS. Peak fractions used for cryo-EM and Thermal Denaturation (TD) assay are delimited by the grey lines (left). SDS-PAGE gel of the pooled SEC fractions of HCN4ΔC, stained with Coomassie blue (right). **E**, Representative SEC of HCN4ΔC – GFP-TRIP8b complex following purification and reconstitution in amphipols. Peak fractions used for cryo-EM are delimited by the grey lines (left). SDS-PAGE gel of the pooled SEC fractions of HCN4ΔC – GFP-TRIP8b complex, stained with Coomassie blue (right). Note that the expected size of the HCN4ΔC and GFP-TRIP8b proteins is the same.

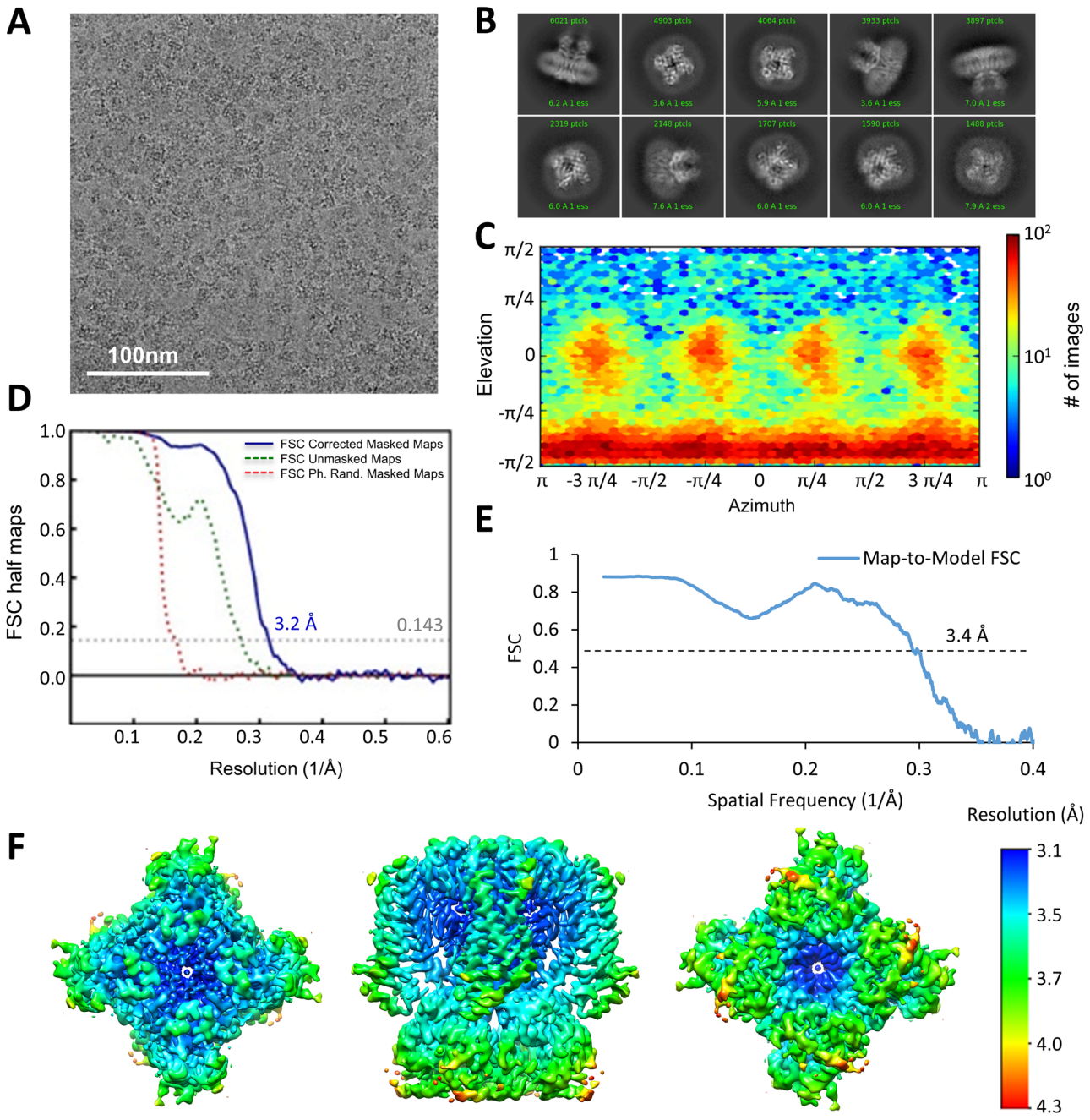

Figure S3: cryo-EM data analysis for cAMP-bound HCN4 (related to Figure 1)
A, Representative micrograph and **B**, 2D classes with box size of 226 Å for cAMP-bound HCN4 in LMNG/CHS (holo). **C**, Heat map of the Euler angle distribution of particle orientations from the final three-dimensional reconstruction in CryoSPARC v.2. **D**, Fourier shell correlation (FSC) curves between the two independently refined half-maps of final cryo-EM 3D reconstruction. **E**, Map to model FSC curves. **F**, Sharpened map of cAMP-bound HCN4 coloured by local resolution.

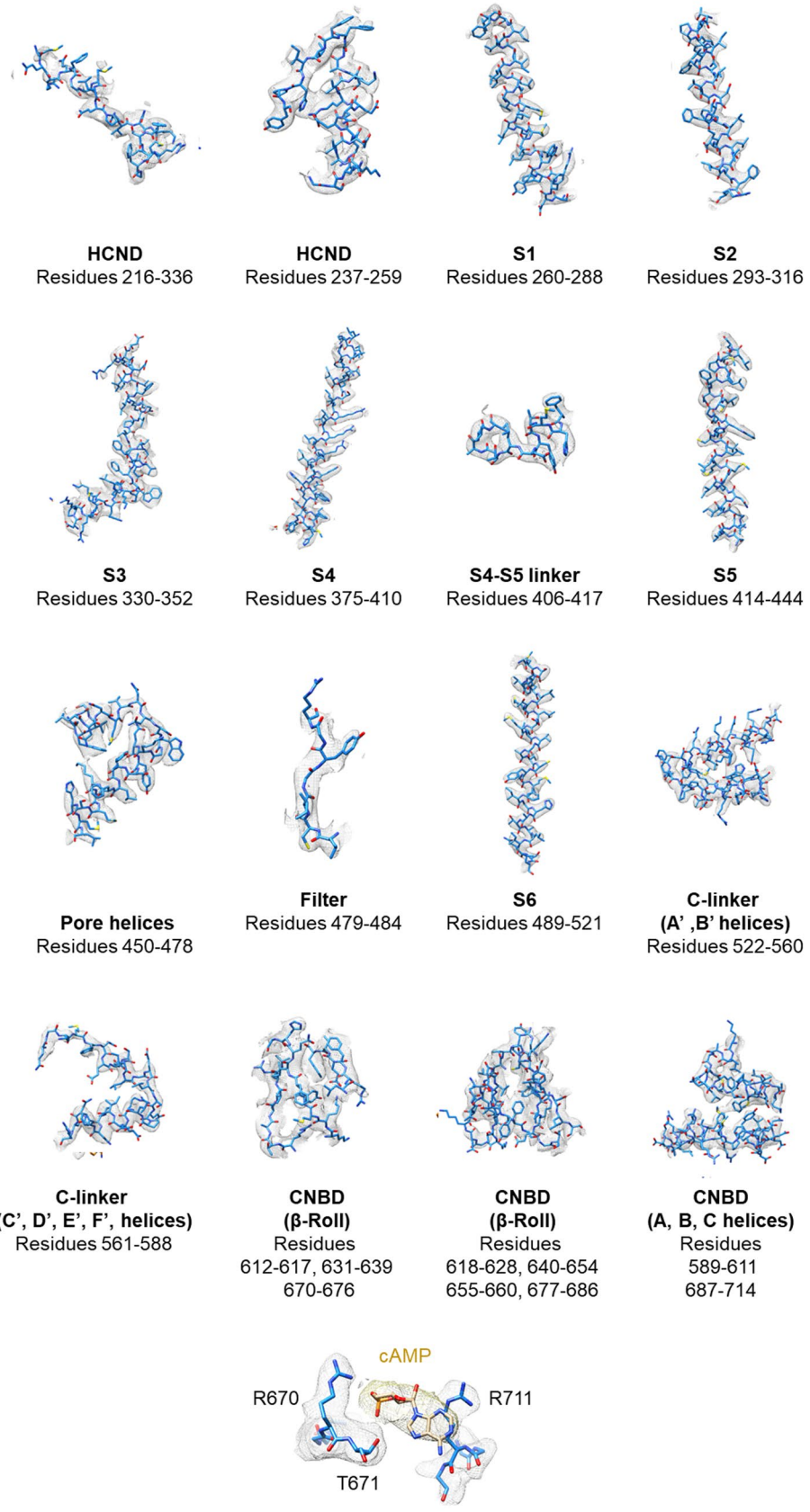

Figure S4: EM density for cAMP-bound HCN4 (related to Figure 1)
Regions of LMNG/CHS solubilized and cAMP-bound HCN4 (holo), as indicated by the figure labels, with model (blue stick) and superimposed density map (grey mesh). The cAMP molecule fitted in its

density (yellow mesh) is also shown, together with the key residues involved in its coordination in the CNBD binding pocket (Zagotta et al., 2003).

Zagotta, W.N., Olivier, N.B., Black, K.D., Young, E.C., Olson, R., and Gouaux, E. (2003). Structural basis for modulation and agonist specificity of HCN pacemaker channels. Nature 425, 200–205.

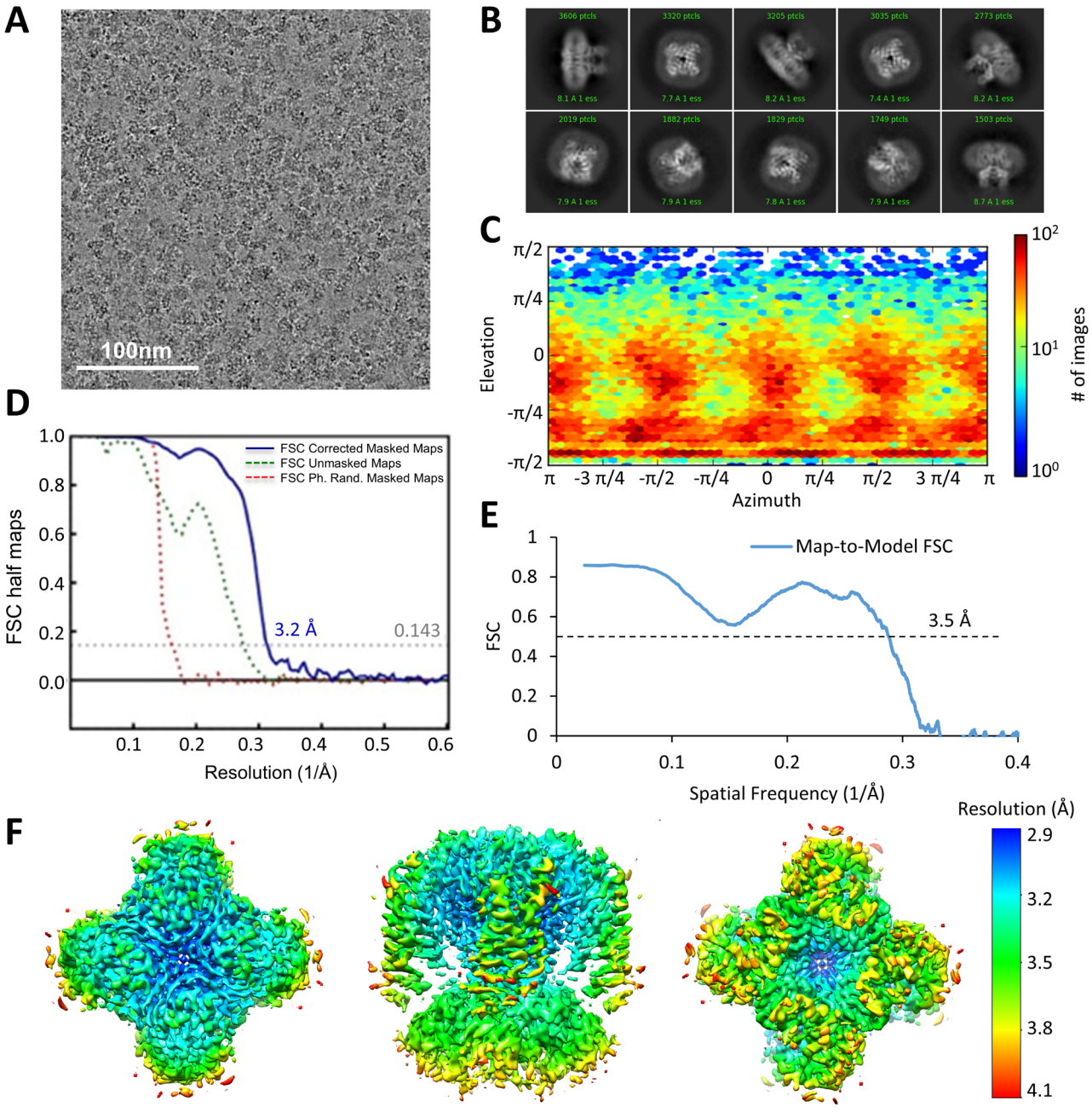

Figure S5: cryo-EM data analysis for apo HCN4 in LMNG/CHS (related to Figure 3)
A, Representative micrograph and **B**, 2D classes with box size of 226 Å for apo HCN4 in LMNG/CHS (apo/LC). **C**, Heat map of the Euler angle distribution of particle orientations from the final three-dimensional reconstruction in CryoSPARC v.2. **D**, Fourier shell correlation (FSC) curves between the two independently refined half-maps of final cryo-EM 3D reconstruction; **E**, Map to model FSC curves. **F**, Sharpened map of apo HCN4 in LMNG/CHS colored by local resolution.

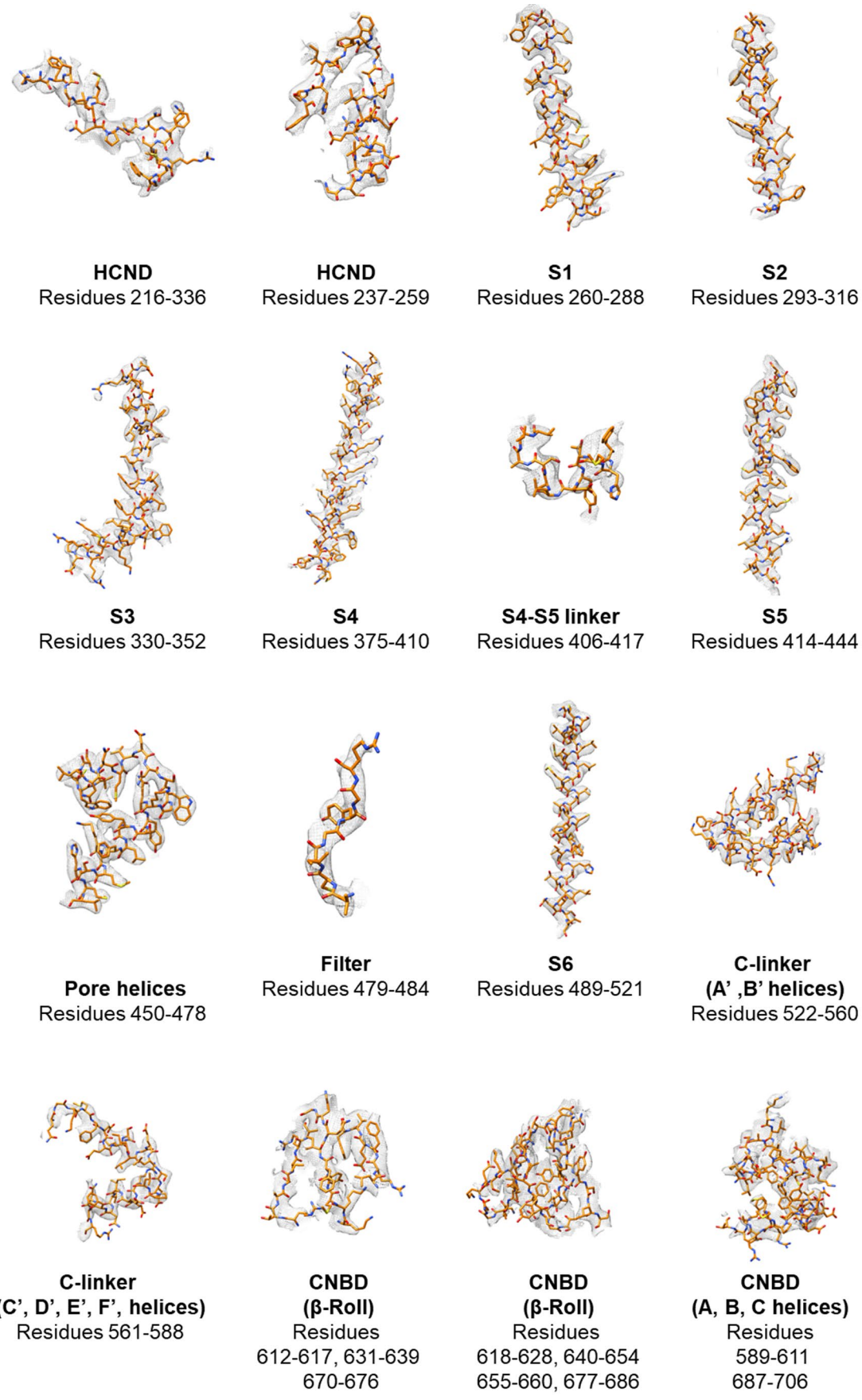

Figure S6: EM density for apo HCN4 in LMNG/CHS (related to Figure 3)
Regions of LMNG/CHS solubilized apo HCN4 (apo/LC), as indicated by the figure labels, with model (orange stick) and superimposed density map (grey me

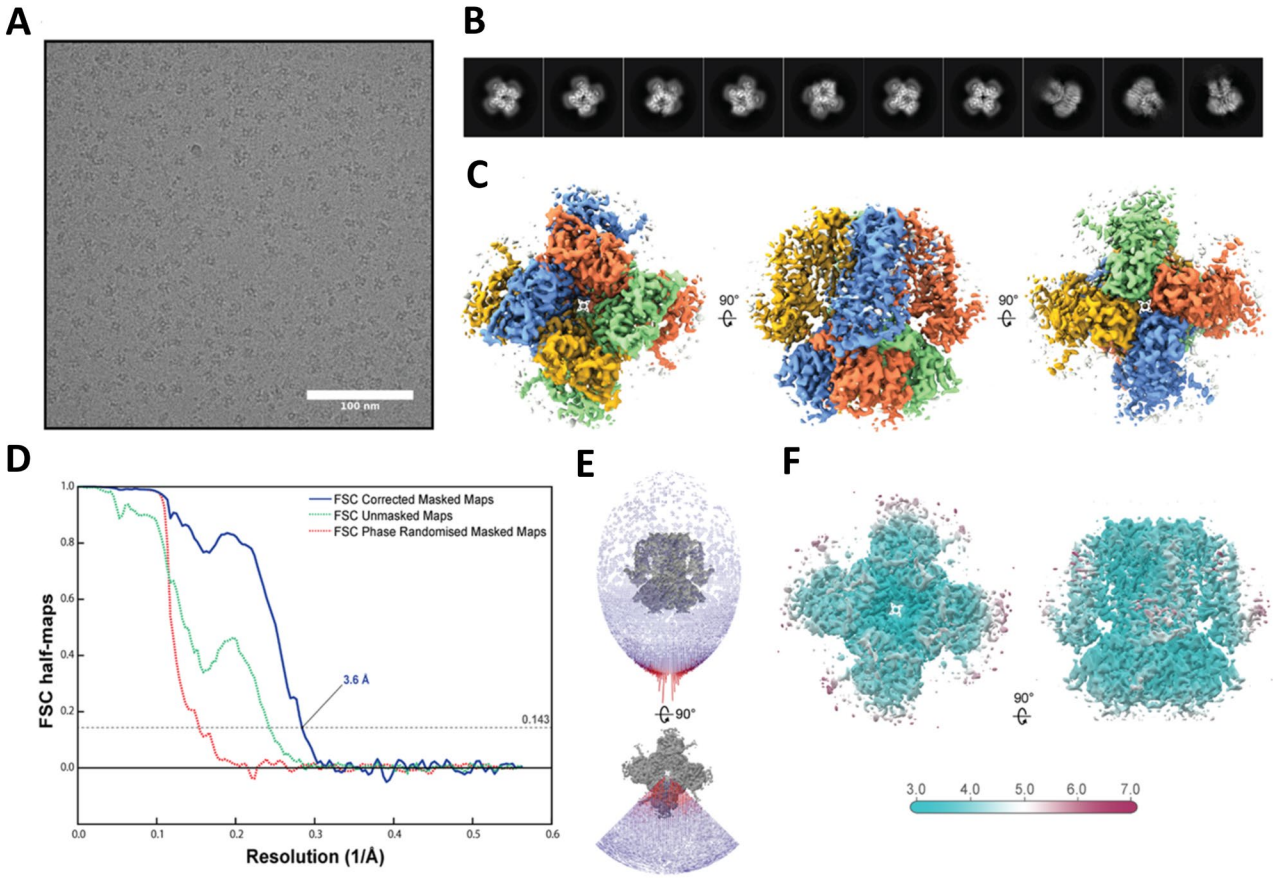

Figure S7: cryo-EM data analysis for apo HCN4 reconstituted into amphipols (related to Figure 4)

A, Representative cryo-EM micrograph of amphipols reconstituted and vitrified apo HCN4 (apo/AM) at estimated defocus of -1.9 µm. **B**, Representative cryo-EM reference-free 2D class averages (box size is 242 Å × 242 Å). **C**, Orthogonal views of the final cryo-EM 3D reconstruction. **D**, Fourier shell correlation curves between the two independently refined half-maps of final cryo-EM 3D reconstruction. **E**, Distribution plot displaying Euler angles of particles used for final cryo-EM 3D reconstruction in Relion. Number of particles contributing to each view is indicated by the color and length of the bar (blue for low number; red for high number). **F**, Orthogonal views of final 3D reconstruction with surface color indicating local resolution estimates.

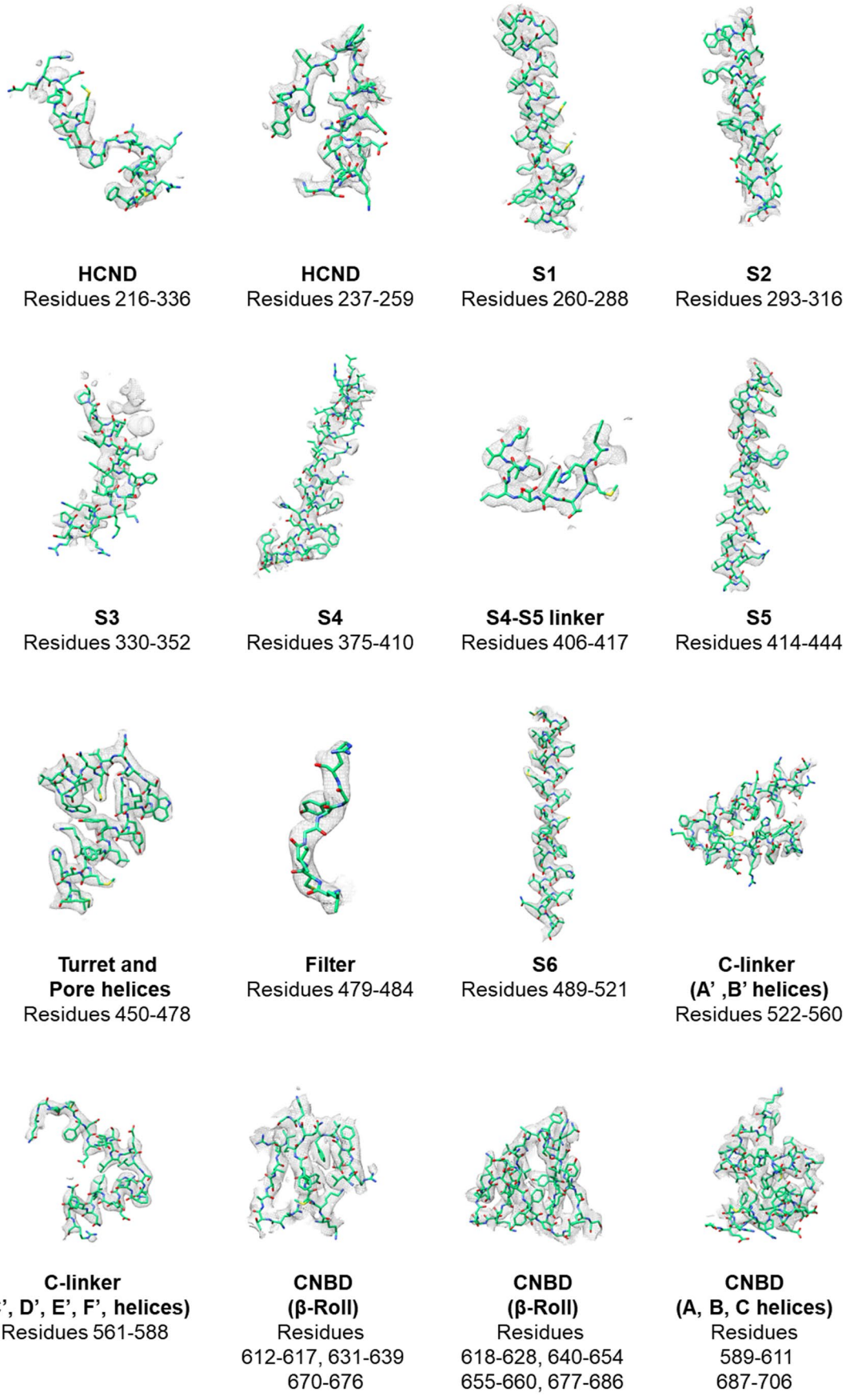

Figure S8: EM density for apo HCN4 reconstituted into amphipols (related to Figure 4)
Regions of amphipols reconstituted apo HCN4 (apo/AM), as indicated by the figure labels, with model (green stick) and superimposed density map (grey mesh).

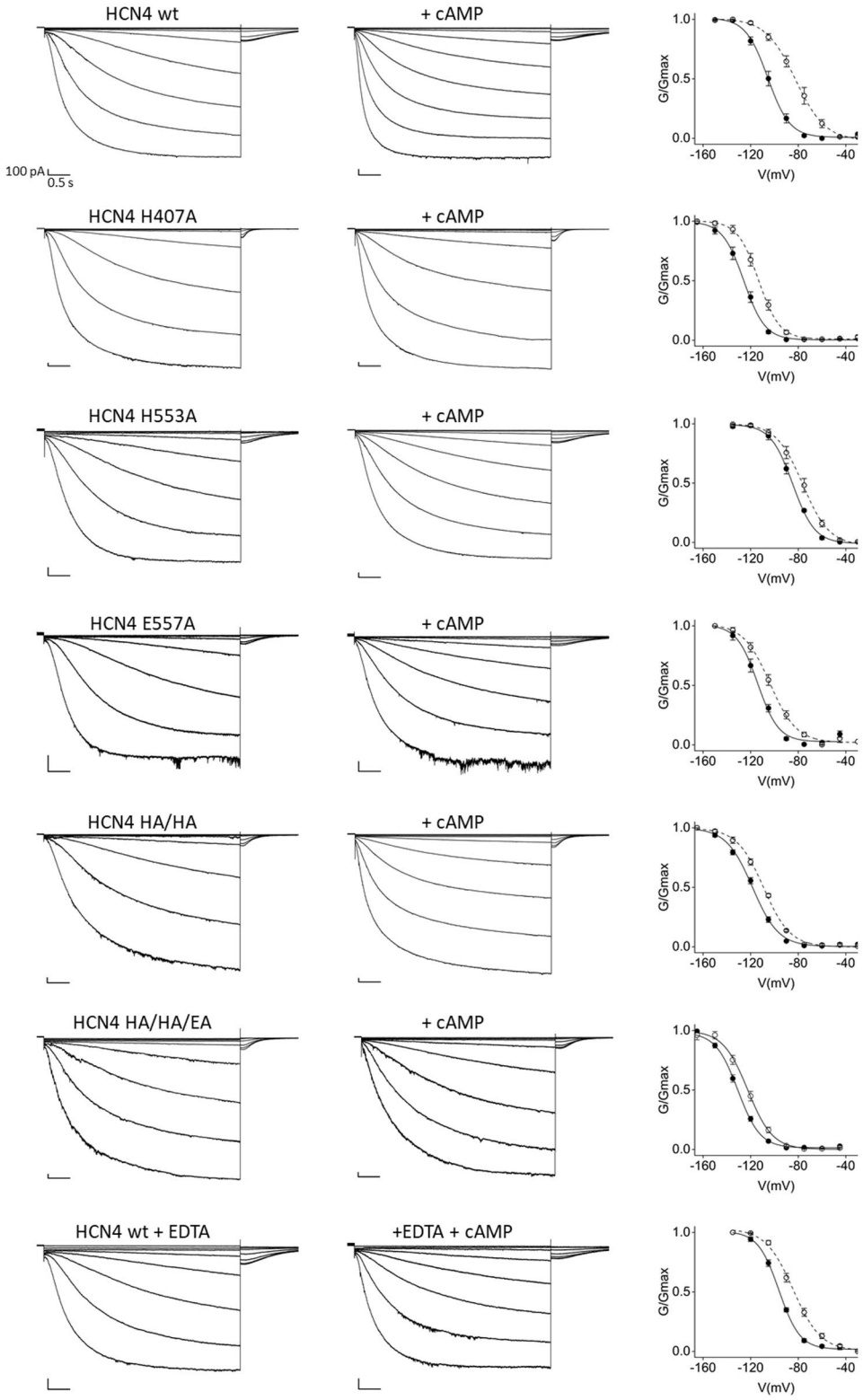

Figure S9: Functional study of the tetrad in HCN4 channels (related to Figure 2).

Left, representative whole-cell currents recorded from HEK293T cells transiently expressing HCN4 wt, and mutant channels in the absence and in the presence of 30 μM cAMP and/or 60 mM EDTA, in the pipette solution. Right, mean activation curves, without (full circles) and with (empty circles) cAMP. Solid lines indicate fitting of the data with a Boltzmann function (see STAR Methods) for determination of half activation potential ($V_{1/2}$) and inverse slope factor (k) values reported in Table S1.

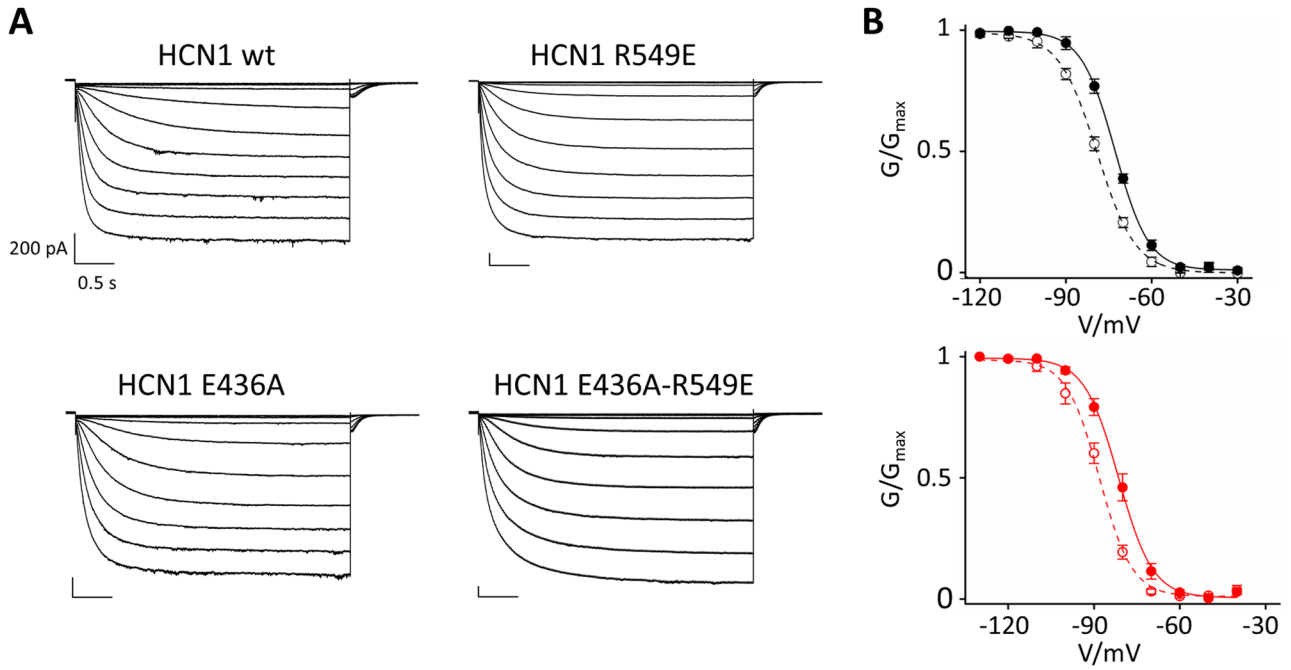

Figure S10: Mutation E436A does not affect cAMP response in HCN1 channels (related to Figure 2)

A, Representative whole cell currents recorded from HCN1 wt and E436A mutant with and without R549E, a mutation that decreases the affinity for cAMP by about 10000 times (Chen et al., 2001). Experiments performed by patch clamp in HEK 293 cells, in whole cell configuration. Voltage protocol is indicated in STAR Methods. Scale bar: 200 pA x 500 ms. **B**, Mean activation curves from the currents in A. In wt channels, (black solid line, top graph) mutation R549E (black dotted line) shifts the half activation voltage ($V_{1/2}$) to the left by 6.1± 0.1 mV indicating that, due to their high affinity for cAMP, HCN1 channels respond to endogenous levels of cAMP present in HEK293T cells (Saponaro et al., 2018). In E436A channels, (red solid line, bottom graph) the comparable size of the left shift in HCN1 R549A and HCN1 E436A-R549A (red dotted line, 7 ± 1 mV) indicates that the cAMP response remains intact in the presence of the E436A mutation. Data are shown as mean ± SEM. Values and statistical analyses are reported in Table S1.

Chen, S., Wang, J., and Siegelbaum, S.A. (2001). Properties of Hyperpolarization-Activated Pacemaker Current Defined by Coassembly of Hcn1 and Hcn2 Subunits and Basal Modulation by Cyclic Nucleotide. J. Gen. Physiol. *117*, 491–504.

Saponaro, A., Cantini, F., Porro, A., Bucchi, A., DiFrancesco, D., Maione, V., Donadoni, C., Introini, B., Mesirca, P., Mangoni, M.E., et al. (2018). A synthetic peptide that prevents cAMP regulation in mammalian hyperpolarization-activated cyclic nucleotide-gated (HCN) channels. Elife *7*.

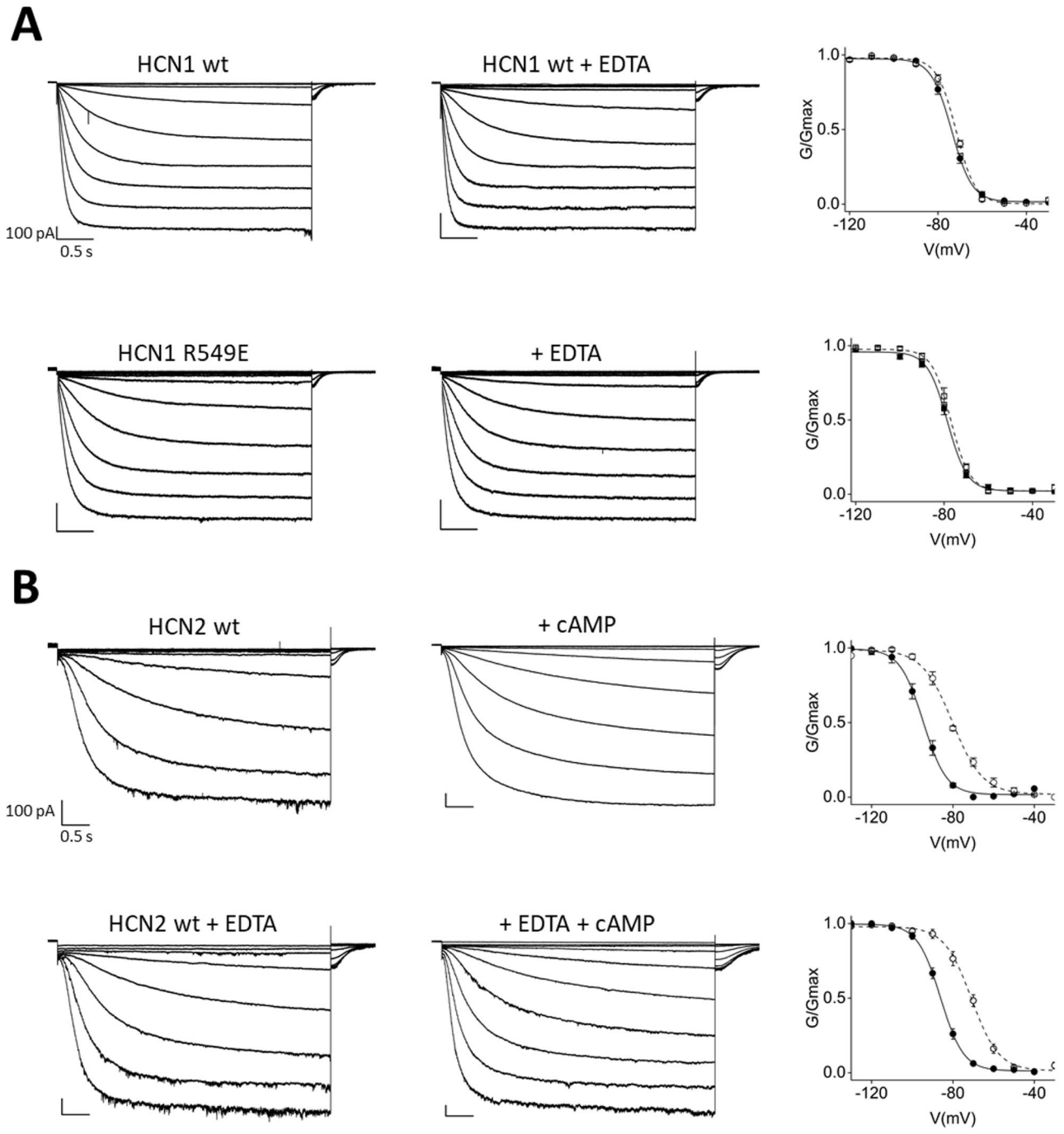

Figure S11: Functional study of the tetrad in HCN1 and HCN2 channels (related to Figure 2).

A, Left, representative whole-cell currents recorded from HEK293T cells transiently expressing HCN1 wt and R549E channels. Right, mean activation curves, without (full circles) and with (empty circles) 60 mM EDTA. **B**, Left, representative whole-cell currents recorded from HEK293T cells transiently expressing HCN2 wt channels in the absence and in the presence of 30 μM cAMP. When indicated, 60 mM EDTA was added to the pipette solution of the experiments. Right, mean activation curves, without (full circles) and with (empty circles) cAMP. **A**, **B**, Lines indicate that fitting of the data with a Boltzmann function (see STAR Methods) that provides half activation potential ($V_{1/2}$) and inverse slope factor (k) values reported in Table S1.

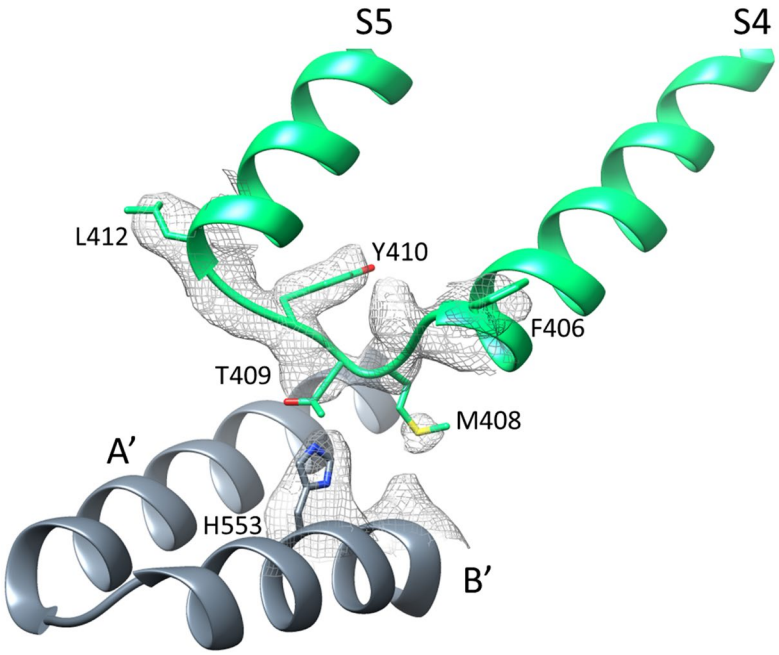

Figure S12: The S4-S5 linker and the underlying C-linker in HCN4 apo/AM structure (related to Figure 3).
Ribbon representation of the S4-S5 linker of one subunit (green) and the C-linker "elbow" (A'-B' helices, grey) of the adjacent subunit of apo/AM HCN4. The density map of the S4-S5 linker and of the two residues of B' helix forming the ion coordination site in HCN4 holo (the tetrad) are shown as grey mesh. Only one of the four residues forming the tetrad (H553) displays enough density to be modelled and is shown as sticks and labelled. Of note, in apo/AM the S5 helix is more tilted compared to apo/LC (S14A) and the helical turn displayed in the S4-S5 linker of both the apo/LC and holo is stretched (Figure S13).

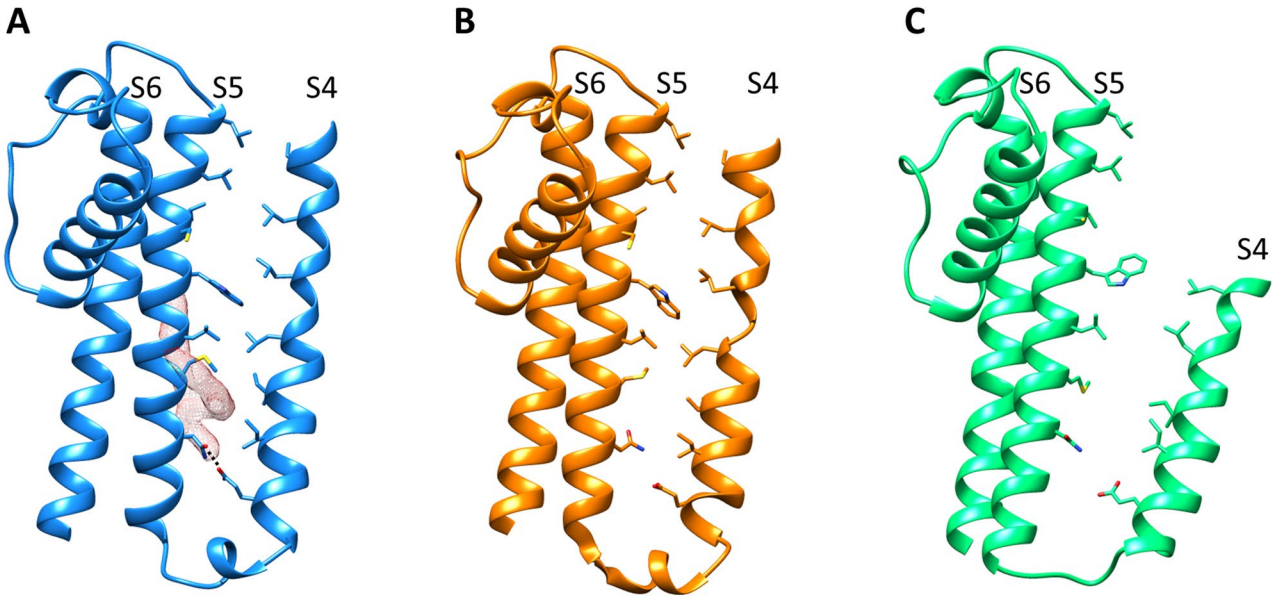

Figure S13: TM helices S4 and S5 are connected by hydrophobic and hydrophilic contacts (related to Figure 4)

Ribbon representation of TM helices S4-S6 of HCN4 holo (blue), apo/LC (orange) and apo/AM (green). **A**, S4 and S5 helices of holo are connected by a zip of interactions formed by the hydrophobic residues of S4 facing towards S5 and vice versa, and by a hydrogen bond between E403 (S4) and N421 (S5). A lipid (red mesh, same as in Figure 4A) embracing S5 contributes to the hydrophobic interaction between S4 and S5. **B**, in apo/LC the hydrophobic interactions formed by the S4 and S5 residues are preserved. Conversely, the lipid and consequently the hydrophobic interactions due to it are absent. The polar contact between E403 and N421 is also absent. **C**, in apo/AM all hydrophobic, polar and lipid contacts are absent and S4 is completely detached from S5.

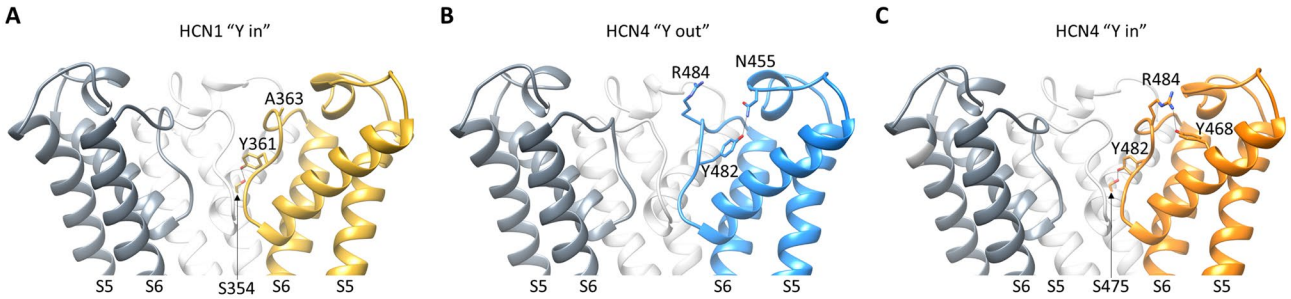

Figure S14: Structural characterization of the two conformations of the HCN4 selectivity filter (related to Figures 4 and 6)

Ribbon representation of the pores shown in side view for HCN1 (**A**, PDB: 5U6P), and HCN4 in the "Y out" (**B**) and "Y in" (**C**) conformation. For clarity only three subunits are shown. Labels indicate TM helix 5 and TM helix 6 (S5, S6). **A**, In the HCN1 "Y in" conformation, Y361 is stabilized by the interaction with S354 from the Pore helix of the white subunit. **B**, in the HCN4 "Y out" conformation, Y482 is stabilized by the interaction with residue N455 of the turret. **C**, In the HCN4 "Y in" conformation, Y482 is stabilized by the interaction with S475 from the Pore helix of the white subunit as it occurs in HCN1 (panel **A**). HCN1 and HCN4 SF differ for one amino acid: A363 in HCN1 (**A**) and R484 in HCN4 (**B, C**). In the HCN4 "Y in" conformation, R484 interacts with Y468 from the Pore helix of the same subunit.

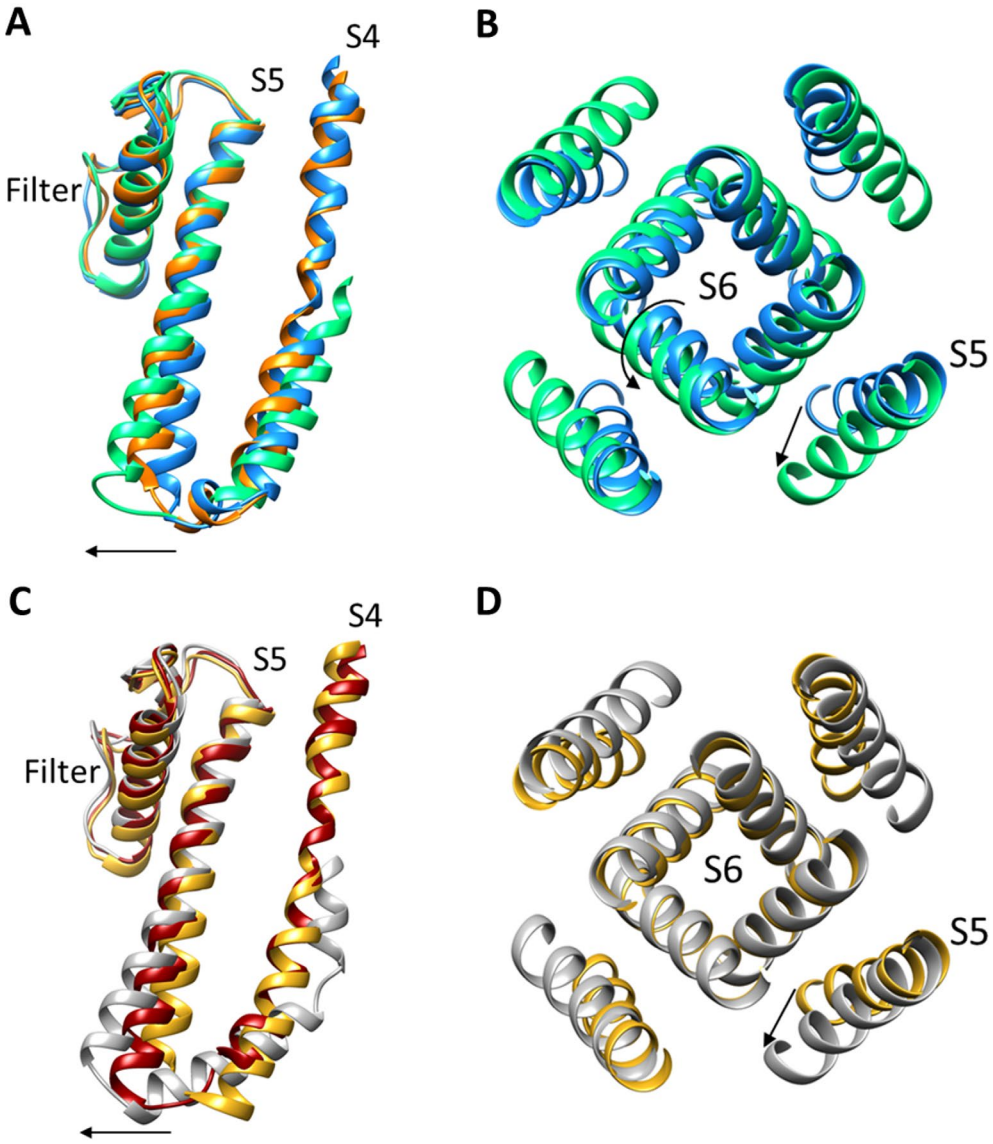

Figure S15: S5 TM helix movements leading to pore opening in HCN4 match those previously observed in HCN1 (related to Figure 4)

A, Superposition of the S4 and S5 TM helices of HCN4 holo (blue), HCN4 apo/LC (orange) and HCN4 apo/AM (green) in a cross-membrane view. For clarity, only one subunit of the tetramer is shown. The black arrow indicates the direction of the movement of the S5 TM helix, whose intracellular end progressively points out of the S4-S6 planar array. **B**, Superposition of the S5 and S6 TM helices of HCN4 holo (blue) and HCN4 apo/AM (green) in a top-down view from the extracellular side of the membrane. The black arrows indicate the direction of the movements of the TM helices. The S5 TM helix tilts upwards, while the S6 TM helix undergoes a rotation and widening at the bundle crossing. **C**, Superposition of the S4 and S5 TM helices of HCN1 holo (yellow, PDB: 5U6P), HCN1 Y289D (dark red, PDB: 6UQG) and HCN1 in the hyperpolarized conformation (grey, PDB: 6UQF) in a cross-membrane view. For clarity, only one subunit of the tetramer is shown. The black arrow indicates the direction of the movement of the S5 TM helix, which progressively tilts out of the S4-S6 planar array. **D**, Superposition of the S5 and S6 TM helices of HCN1 holo (yellow, PDB: 5U6P) and HCN1 in the hyperpolarized conformation (grey, PDB: 6UQF) in a top-down view. The black arrows indicate the direction of the movement of the S5 TM helix tilting upwards. Contrary to HCN4, in HCN1 the S6 TM helices do not move.

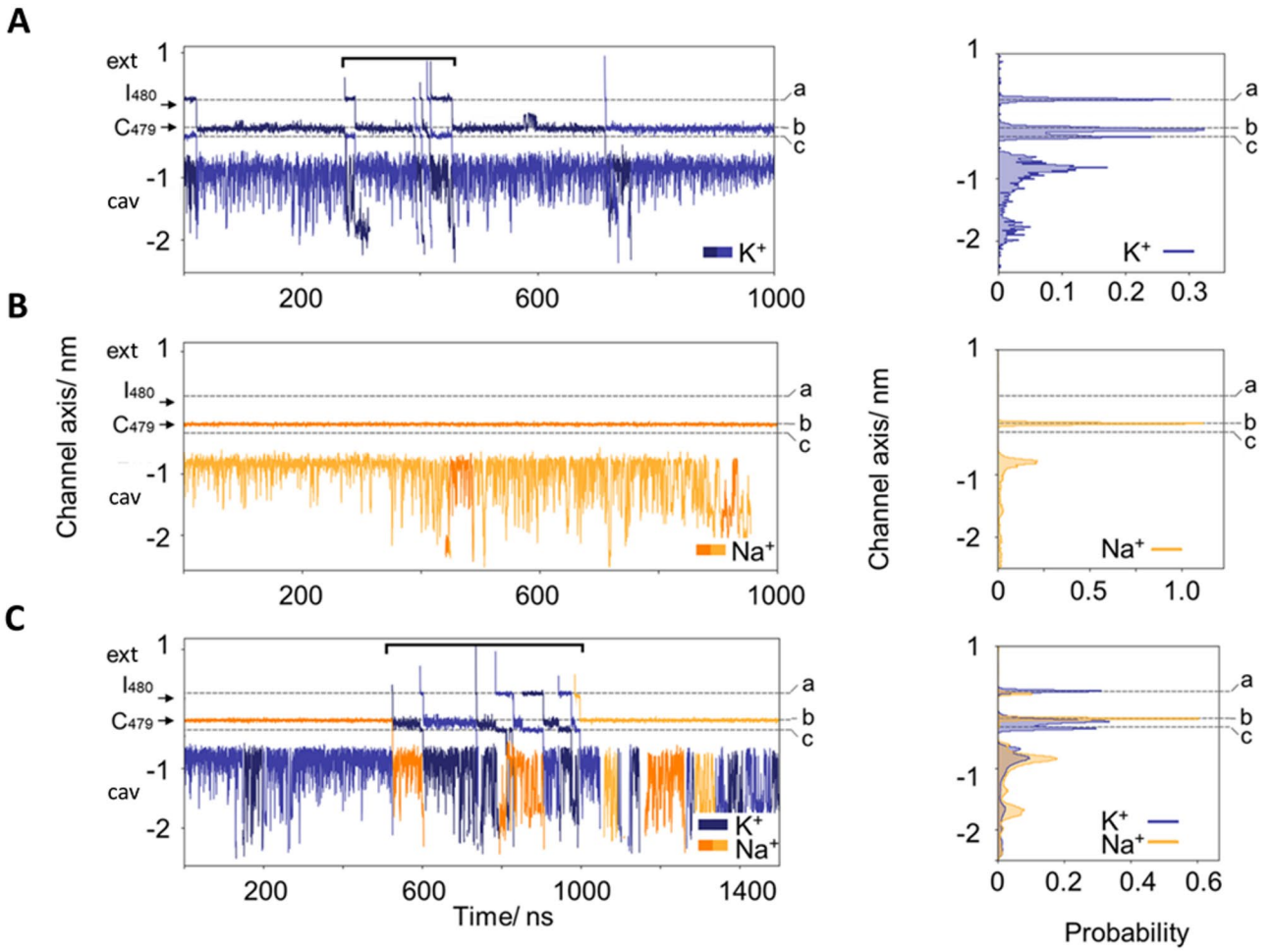

Figure S16: Full MD trajectories and ion density profiles (related to Figure 6)
Full trajectories of ions in the SF (left) and ion density profiles along the channel axis (right) in MD simulations in **A**, KCl, **B**, NaCl and **C**, equimolar KCl and NaCl. K^+ ions and Na^+ ions are shown in different shades of blue and orange, respectively. Dashed horizontal lines mark the positions a,b,c of the ions identified in Figure 6. Arrows indicate carbonyl oxygen atoms of residues 479-480 and the labels ext and cv mark the extracellular side and the cavity, respectively. Black parentheses in (A) and (C) mark the region shown in Fig 6B and D.

Table S1: Numerical values for parameters from patch clamp experiments performed on HCN channels expressed in HEK293T cells (related to Figure 2, S2 and S9-11).

	$V_{1/2}$ (mV) ± SEM Control	k (mV) ± SEM Control	n	$V_{1/2}$ (mV) ± SEM + 30 µM cAMP	k (mV) ± SEM + 30 µM cAMP	n	cAMP-induced $V_{1/2}$ shift ± SEM
HCN4 wt	- 102.6 ± 0,7	10.6 ± 1.2	4	- 81.9 ± 1.5 §	11.2 ± 0.6	5	20.7 ± 1.6
HCN4 ΔC	- 101.3 ± 1,6 n.s.	12.1 ± 0.45	5	- 70.3 ± 0.9 §	9.5 ± 0.3	4	31 ± 1.8 *
HCN4 wt	- 102.8 ± 1	9.1 ± 1.2	15	- 85 ± 1.2	9.4 ± 0.7	17	17.8 ± 1.6
HCN4 H407A	- 126 ± 2 *	8.8 ± 0.8	7	- 114 ± 2 §	8.9 ± 0.6	7	12 ± 2.8 *
HCN4 E557A	- 114 ± 1.9 *	9.1 ± 1	3	- 104.5 ± 1.7 §	11.6 ± 0.8	5	10 ± 2.6 *
HCN4 H553A	- 84 ± 0.9 *	9.4 ± 0.9	4	- 77.0 ± 2.5 §	11.1 ± 1.1	6	7 ± 2.7 *
HCN4 H407A-H553A	- 118.8 ± 1.2 *	10.9 ± 0.5	11	- 109.7 ± 1 §	11.5 ± 0.7	8	9.1 ± 1.5 *
HCN4 H407A-H553A-E557A	- 132 ± 1.1 *	10 ± 0.3	10	- 124.4 ± 2 §	11.3 ± 0.4	7	7.6 ± 2.3 *
HCN4 wt with EDTA	- 96.6 ± 0.7 *	9.1 ± 0.5	8	- 85.6 ± 1.37 §	10.2 ± 0.7	6	11± 1.55 *
HCN1 wt	- 73.2 ± 0.6	4.6 ± 0.6	13	n.t.	n.t.	-	5.8 ± 0.9 (#)
HCN1 R549E	- 79 ± 0.7 *	4.3 ± 0.6	11	n.t.	n.t.	-	
HCN1 E436A	- 81.4 ± 1.3 *	5.8 ± 0.4	5	n.t.	n.t.	-	7 ± 1 n.s. (#)
HCN1 E436A-R459E	- 88.4 ± 1.1 *	5.9 ± 0.9	7	n.t.	n.t.	-	
HCN1 wt with EDTA	- 71.8 ± 0.5 *	4.5 ± 0.7	6	n.t.	n.t.	-	5.2 ± 1.1 (#)
HCN1 R549E with EDTA	- 77 ± 1 *	4.2 ± 0.9	5	n.t.	n.t.	-	
HCN2 wt	- 94.7 ± 1.5	6.1 ± 0.5	6	- 80.7 ± 0.3 §	6.5 ± .08	5	14 ± 1.5
HCN2 wt with EDTA	- 86 ± 1 *	6.3 ± 1.0	7	- 71.0 ± 1.3 §	7.0 ± 1.2	7	15 ± 1.6 n.s.

Fitting parameters of the activation curves in HCN4, HCN1 and HCN2 channels.

Half-activation voltage ($V_{1/2}$) and inverse slope factor (k) obtained by fitting data to a Boltzmann function (see STAR Methods) in absence or presence of cAMP (30 µM or 15 µM for HCN4 and HCN2 respectively); n= number of cell tested in each condition.

*$p<0.05$ by One-way ANOVA with Fisher's test compared to wt HCN4, HCN1 or HCN2; §$p<0.05$ by Student's T-test compared to control condition (without cAMP); n.s. not statistically different; n.t. not tested.

(#) In HCN1 channels, the shift induced by cAMP was calculated by comparing their $V_{1/2}$ with those obtained introducing the R549E mutation, which is known to reduce the affinity for cAMP by about 1000 times (Chen et al, 2001b); for details see legend of Figure S9.

Table S2: Activation and deactivation time constants of HCN4 wt and ΔC channels expressed in HEK293T cells (related to Figure S2).

V/mV		HCN4 wt	HCN4 ΔC
-105	τ activation (s)	4.5 ± 0.75	4.2 ± 0.2$^{n.s.}$
-120		2.0 ± 0.10	1.8 ± 0.2$^{n.s.}$
-135		1.1 ± 0.07	1.0 ± 0.06$^{n.s.}$
-150		0.6 ± 0.04	0.7 ± 0.07$^{n.s.}$
-40	τ deactivation (s)	0.66 ± 0.03	0.64 ± 0.02$^{n.s.}$

Activation and deactivation time constants (τ) were obtained by fitting raw traces to a single exponential function (see STAR Methods). Data were compared by Student's T-test. n.s. not statistically different.

Table S3: Details of MD simulations (related to Figure 6).

Simulation	Pure K^+	Pure Na^+	1:1 K^+:Na^+
K^+	229	-	114 to 124
Na^+	-	229	115 to 124
Ion concentration (mM)	900	900	450:450
#Water	13,823 to 13,824	13,823 to 13,824	13823 to 14,778
#Lipids	202	202	182 to 202
Transmembrane Voltage (mM)	-500	-500	-500 to -700
Statistics			
# Independent Simulations	4	5	15
Total simulation time (ns)	2,100	4,500	7,600
Simulations w/ conduction	2	0	7
Simulation w/o conduction	2	5	8
Permeation			
K^+	9	-	11
Na^+	-	0	4
Water	9	0	15
Permeation ratio (water/ions)	1.0	1.0	1.0
Selectivity			
K^+ replacing K^+	9	-	7
K^+ replacing Na^+	-	-	3
Na^+ replacing K^+	-	-	4
Na^+ replacing Na^+	-	0	1